Published in Analytica Chimica Acta 633, issues 1-2, 175-181, 2008
which should be used for any reference to this work

Computer simulation and theory of the diffusion- and flow-induced concentration dispersion in microfluidic devices and HPLC systems based on rectangular microchannels

Werner E. Morf[1], *Peter D. van der Wal**, *Nicolaas F. de Rooij*

SAMLAB, Institute of Microtechnology (IMT), University of Neuchâtel, CH-2000 Neuchâtel, Switzerland

A B S T R A C T

The dynamics of formation of solute peaks in microfluidic systems are investigated by computer simulation. A finite-element numerical procedure is applied to analyze the diffusion- and flow-controlled concentration dispersion in a 40 μm-high rectangular flow-through channel. Two-dimensional concentration profiles are shown for channels with cross sections of large aspect ratio. The final shapes of the peaks are formed during a very short time period, ranging from a few milliseconds to about 1 s for low and high flow velocities, respectively. The observed standard half-width σ of the peaks is found to strictly follow a linear function of $t^{1/2}$ over the whole time range. The extrapolated long-term peak characteristics are in perfect agreement with theoretical predictions. For comparison, theoretical results on the concentration dispersion for solute peaks in open-channel liquid-chromatography (HPLC) are re-examined and applied.

Keywords: Microfluidic system, Chromatography, Rectangular channel, Concentration dispersion, Peak profile, Computer simulation, Finite-difference method, Theory

1. Introduction

In the past years, microfabricated flow-through devices continued to be of utmost relevance with respect to research, development, and application [1,2]. For analytical–chemical purposes, micro-total-analysis systems [3,4] (μ-TAS, lab-on-a-chip; for a review see [5–11]) and other microfluidic systems [12,13] have been introduced as highly promising and extremely useful tools. A common feature of most of these devices is that they essentially consist of microchannels in which the analyte solution is transferred either hydrodynamically by an applied pressure difference, or electroosmotically by an electrical potential gradient.

Pressure-driven open-tubular microsystems have the potential for considerable innovations and improvements, for instance, in the area of high-performance liquid chromatography (HPLC) [14]. In these systems, zones of solute components are transported in the mobile phase, separated by distribution between the mobile phase and the stationary phase (formed by a retentive coating on the channel wall), and finally ana-

lyzed by a detector unit. Obviously, the performance of such analytical determinations is directly related to the concentration dispersion of the solute peaks and is therefore limited by diffusion and flow processes. Such influences in open-tubular chromatography have been treated theoretically first by Taylor [15] and Golay [16,17]. The corresponding results have been generally adopted for flow-through systems based on different channel types [18–24]. Microfabricated devices usually incorporate channels that roughly have a rectangular cross-section. The performance of rectangular chromatographic columns has been analyzed first by Golay [16] (see also [21]), and was studied extensively in recent contributions [25–33]. In addition to theoretical treatments, numerical modeling of mass transfer has proved to be successful in tracing down the performance of such columns [33–37].

More insight into the evolution of solute peaks in microchannels can be gained from computer simulations that model the underlying mass-transport and convective processes by numerical methods. Here, we present results of a finite-element modeling of diffusion and flow processes in rectangular microfluidic channels. The aim of these virtual experiments was to analyze the dynamics of peak formation. Two-dimensional concentration distributions are determined for channels of large aspect ratio. It will be shown that the long-term peak profiles extrapolated from these data agree with the performance predicted from theory. For comparison, the key results of Golay's theory on chromatography are re-examined.

2. Theoretical section

The channels treated in this work have the idealized shape of a rectangular parallelepiped with the coordinate x ranging from $-h/2$ to $h/2$, the coordinate y from $-w/2$ to $w/2$, and the coordinate z from 0 to l, where h, w, and l are the height, the width, and the length, respectively. In the case of HPLC systems, the channel walls are formed by a retentive stationary phase, which is assumed to be a homogeneous film of thickness δ. A hydraulic flow moving in the z-direction through such a channel can be considered as a purely laminar flow of the mobile phase which is assumed to be an incompressible solution. When a zone of a solute component is injected, distinct diffusion processes and convection influences give rise to a distortion of the zone and to a broadening of the concentration distribution with increasing time t.

In the present study, computer simulations for rectangular channels are used to analyze the effects of concentration dispersion by longitudinal diffusion in the z-direction, by lateral diffusion in the x-direction, as well as by convection in the z-direction. For simplicity, a parallel-plate geometry with $w \gg h$ is assumed, which implies that the velocity profile in the mobile phase becomes completely flat along the y-axis, except for the two boundary layers near the walls at $y = -w/2$ and $y = w/2$ [27,38,39]. In fact, the average flow velocity in a rectangular channel of the width $w = 10h$ differs by only 6% from that in an infinitely wide channel of the same height h at the same pressure [40]. Convection-induced diffusion fluxes in the y-direction will therefore be neglected, as a first-order approximation, for channels of very large aspect ratio (parallel-plate or slab geometry). Accordingly, the fundamental differential equation of diffusion and convection in the mobile phase is given by Eq. (1):

$$\frac{\partial c}{\partial t} = D\frac{\partial^2 c}{\partial x^2} + D\frac{\partial^2 c}{\partial z^2} - v(x)\frac{\partial c}{\partial z} \tag{1}$$

where c is the concentration and D is the molecular diffusion coefficient of a solute species in the mobile phase, and v is the local linear flow velocity depending on the coordinate x. It is assumed that the solute particles are small in comparison with the channel height and that D can be treated as flow-independent. It should be noted that the combination of the first and the third term accounts for the convection-induced dispersion, in analogy to Taylor's formulation for cylindrical channels [15]. The velocity profile for the flow of the mobile phase between two parallel plates of length l that are separated by the distance h is described by [38,41]:

$$v(x) = 1.5v_0\left(1 - \frac{4x^2}{h^2}\right) \quad \text{with} \quad v_0 = \frac{\Delta p h^2}{12\eta l} \tag{2}$$

where v_0 is the average linear flow velocity, Δp the pressure difference applied along the z-axis, and η is the viscosity of the mobile phase. Because of the retention by the stationary phase, the solute component moves at a reduced average velocity $v_0(1+k)^{-1}$, where k is the capacity factor that depends on the distribution coefficient K of the solute and on the total volume ratio $2\delta/h$ (for $w \gg h$) between the stationary phase of thickness δ and the mobile phase of height h:

$$k = \frac{2\delta}{h}K \tag{3}$$

Accordingly, a more convenient version of the continuity equation, Eq. (1), is obtained after transformation of the coordinate z into $\zeta = z - v_0(1+k)^{-1}t$, which results in a concentration distribution centered at $\zeta = 0$ [16] (see below):

$$\frac{\partial c}{\partial t} = D\frac{\partial^2 c}{\partial x^2} + D\frac{\partial^2 c}{\partial \zeta^2} - v(x)\frac{\partial c}{\partial \zeta} + v_0\frac{1}{1+k}\frac{\partial c}{\partial \zeta} \tag{4}$$

The diffusion of the solute species in the convection-free stationary phase can be described by an analogous expression after transformation of the coordinate z into ζ:

$$\frac{\partial c_s}{\partial t} = D_s\frac{\partial^2 c_s}{\partial x^2} + D_s\frac{\partial^2 c_s}{\partial \zeta^2} + v_0\frac{1}{1+k}\frac{\partial c_s}{\partial \zeta} \tag{5}$$

where c_s is the concentration and D_s is the diffusion coefficient of the component in the stationary phase (i.e., for $h/2 \le x \le h/2 + \delta$).

Golay [16,17] solved the differential equations in Eqs. (4) and (5) by making use of the appropriate boundary conditions for open-tubular chromatography (see also [21]). He derived a basic relationship for the average concentration c_{av} in the mobile phase at the location ζ:

$$c_{av} = \frac{2}{h}\int_0^{h/2} c(x)dx \tag{6}$$

which may be written as:

$$\frac{\partial c_{av}}{\partial t} = D^* \frac{\partial^2 c_{av}}{\partial \zeta^2} \tag{7}$$

$$D^* = D\frac{1}{1+k} + D_s\frac{k}{1+k} + \frac{v_0{}^2h^2}{420D}\frac{2+18k+51k^2}{(1+k)^3} + \frac{v_0{}^2\delta^2}{3D_s}\frac{k}{(1+k)^3} \tag{8}$$

Eq. (7) is formally identical to the one-dimensional diffusion equation although the apparent overall dispersion coefficient D^* evidently accounts for longitudinal diffusion in the mobile and the stationary phase (first two terms in Eq. (8)) as well as for convection-influenced lateral diffusion in the two phases (last two terms in Eq. (8)). Finally, the following result for the concentration profile of the solute peak is established, in analogy to the classical solution for diffusion from a plane source [42]:

$$c_{av}(\zeta, t) = \frac{M}{\sqrt{2\pi}\sigma}\exp\left(\frac{-\zeta^2}{2\sigma^2}\right) \tag{9}$$

$$\sigma^2 = 2D^*t \tag{10}$$

where $M = n_{in}/A$ is the mole number n_{in} of solute that is initially present at $z = 0$ in the cross section area $A = hw$ of the channel, and σ^2 is the total dispersion-induced length variance of the concentration distribution after the time t. Eq. (9) evidently predicts a Gaussian peak profile with the standard half-width σ.

A key result follows for the height equivalent to a theoretical plate, HETP [18–21], which is obtained in the general form [16,21]:

$$\mathrm{HETP} = \frac{2D}{v_0} + \frac{2D_sk}{v_0} + \frac{v_0h^2}{210D}\frac{2+18k+51k^2}{(1+k)^2} + \frac{2v_0\delta^2}{3D_s}\frac{k}{(1+k)^2} \tag{11}$$

Again contributions from longitudinal diffusion in z-direction are considered for the mobile and the stationary phase (first two terms), as well as contributions from convection-induced lateral diffusion in x-direction for both phases (last two terms). Eq. (11) is very similar to the result for cylindrical tubes of radius R [16,21]:

$$\mathrm{HETP} = \frac{2D}{v_0} + \frac{2D_sk}{v_0} + \frac{v_0R^2}{24D}\frac{1+6k+11k^2}{(1+k)^2} + \frac{2v_0\delta^2}{3D_s}\frac{k}{(1+k)^2} \tag{12}$$

Eqs. (11) and (12) formally correspond to the van-Deemter–Golay equation [16–18]. It should be pointed out that earlier derivations did not account for longitudinal diffusion in the stationary phase (second term). However, this contribution turns out to be a logical extension of the classical theory since the solute species spend only a part $(1+k)^{-1}$ of the total retention time in the mobile phase, but a k-times longer period in the stationary phase. Accordingly, the respective term cannot be neglected *a priori*, except for gas chromatographic columns where D is much larger than D_s. For HPLC systems with $k \gg 1$, on the other hand, the first two contributions to HETP may even be of the same order of magnitude. Eqs. (11) and (12) evidently differ from each other in the third term that arises from the convection-induced lateral diffusion in the mobile phase. In the case of HPLC systems with $k \gg 1$, the corresponding contribution for a rectangular channel of height h is 2.12 times larger than for a cylindrical capillary of diameter $2R = h$. Accordingly, the standard half-width σ of solute peaks in the rectangular channel may be about 1.5 times larger than in the cylindrical capillary. In all other respects, however, the two channel types exhibit an equivalent behavior.

In the literature several modifications or extensions of Eq. (11) have been reported that rely on different approximations or boundary conditions [25–33]. It has been shown that additional contributions to HETP are generated at the side-walls of rectangular channels when these channels have a finite width [25–33]. The recent work also led to some confusion about the channel geometry treated in Golay's original paper [16]. It must be emphasized that the derivation of Eq. (11) is clearly based on the velocity profile in Eq. (2) (see Eq. (32) in [16]). Therefore, Eq. (11) holds for a rectangular channel of very large aspect ratio (parallel-plate or slab geometry: $w \gg h$), and not for a square column ($w = h$) as suggested recently [26,33]. It should also be mentioned that Golay's theory does not apply to the domain of very high flow velocities since the derivation neglects any higher order terms [16]. Actually, additional contributions to HETP were observed in some cases. Pai et al. proposed a dispersion-convolution model for simulating peaks in flow-injection systems and used an empirical correlation of the type $D^* = \kappa_1 + \kappa_2 v_0 + \kappa_3 v_0^2$ for the dispersion coefficient [37]. This would also yield a second-order equation for HETP where, compared with Eqs. (11) and (12), an additional, flow-independent term would arise.

In the following, non-chromatographic flow-through channels without solute retention are investigated. Here Eqs. (8), (10), and (11) yield a much simpler description:

$$\sigma^2 = 2Dt + \frac{v_0^2h^2t}{105D} \quad (\text{for } k = 0) \tag{13}$$

$$\mathrm{HETP} = \frac{2D}{v_0} + \frac{v_0h^2}{105D} \quad (\text{for } k = 0) \tag{14}$$

Eq. (14) predicts a minimal value, $\mathrm{HETP} = 0.276h$, being reached for $v_0 = 14.5D/h$. The corresponding flow velocity is given by $0.036\,\mathrm{cm\,s^{-1}}$ when a diffusion coefficient D of $10^{-5}\,\mathrm{cm^2\,s^{-1}}$ and a channel height h of 40 μm are assumed. The computer simulations reported below refer to flow conditions near this minimum. It will be shown that Eqs. (13) and (14) offer an excellent description of the long-term peak characteristics for rectangular microfluidic channels.

3. Computer simulations

Computer simulations of diffusion and convection processes were performed in order to study the dispersion of solute concentrations in rectangular microfluidic channels. These virtual experiments permit it to immediately observe the evolution of peaks with time and to compare the found con-

centration profiles with the theoretical results of Section 2. Appropriate finite-difference procedures were developed earlier for numerical simulations of solute fluxes in aqueous and membrane systems [43–45]. In the present case, the diffusive and convective transport processes were analyzed in the x–z-plane, where x is the height coordinate and z is the length axis of the channel. Concentration and velocity changes in the y-direction were neglected according to the former approximation for sufficiently wide channels. The x-range, given by an assumed channel height of $h = 40\,\mu m$, was segmented into 39 inner elements of 1 μm thickness and 2 half-elements for the boundaries. The studied z-range, a 100 μm long section of the whole channel length, was also subdivided into elements of 1 μm thickness. This made it possible to replace the differentials in the basic Eq. (1) by finite differences between the centers of neighbouring elements [43–45]:

$$\frac{\Delta c_{n,p}}{\Delta t} = D\frac{c_{n-1,p} - 2c_{n,p} + c_{n+1,p}}{\Delta x^2} + D\frac{c_{n,p-1} - 2c_{n,p} + c_{n,p+1}}{\Delta z^2} + v_n\frac{c_{n,p-1} - c_{n,p}}{\Delta z} \quad (15)$$

where n and p are the numbers of a given element on the x- and z-axis, respectively, $\Delta c_{n,p}$ the concentration change in this element during a short time interval Δt, $\Delta x = \Delta z = 1\,\mu m$ the length of each element, and v_n is the flow velocity in the n-th element on the x-axis (see Eq. (2)). The diffusion coefficient D was taken as $10^{-5}\,cm^2\,s^{-1}$, and the average flow velocity v_0 ranged from 0.015 to 0.08 cm s^{-1}. For the half-elements with $n = 1$ and $n = 41$, the boundary condition $c_{n-1,p} = c_{n+1,p}$ due to zero lateral fluxes [44] was used in Eq. (15).

Based on this procedure, the diffusion- and convection-induced concentration changes in the channel were evaluated for time steps of $\Delta t = 0.01$ ms. It was assumed that the solute is initially present in the elements with $p_0 = 21$ at a concentration $c_{in} = n_{in}/A\Delta z$, where n_{in} is the mole number in the initial volume $A\Delta z$. Finally, the evolution of the peak profile could be analyzed in the space and time domains and was compared with theoretical results according to Eq. (9), written in the form:

$$c_{av}(p, t) = c_{in}\frac{\Delta z}{\sqrt{2\pi\sigma}}\exp\left[-\frac{(p\Delta z - p_0\Delta z - v_0 t)^2}{2\sigma^2}\right] \quad (16)$$

where c_{av} is the average concentration of all elements n at a given position p on the z-axis, and σ is the standard half-width of the peak. The numerical calculations were performed with conventional MS Excel software (Microsoft Corp.) in order to guarantee the maximum transparency of the mathematical procedure.

4. Results and discussion

The above finite-difference procedures were applied to study the dynamics of peak formation in rectangular microfluidic channels of large aspect ratio. The development of time-dependent concentration distributions, starting from a 1 μm broad zone of solute in the elements with $p_0 = 21$ at $t = 0$, is illustrated in Figs. 1 and 2. Results are shown for flow velocities v_0 of 0.04 and 0.06 cm s^{-1}, respectively, and for time intervals

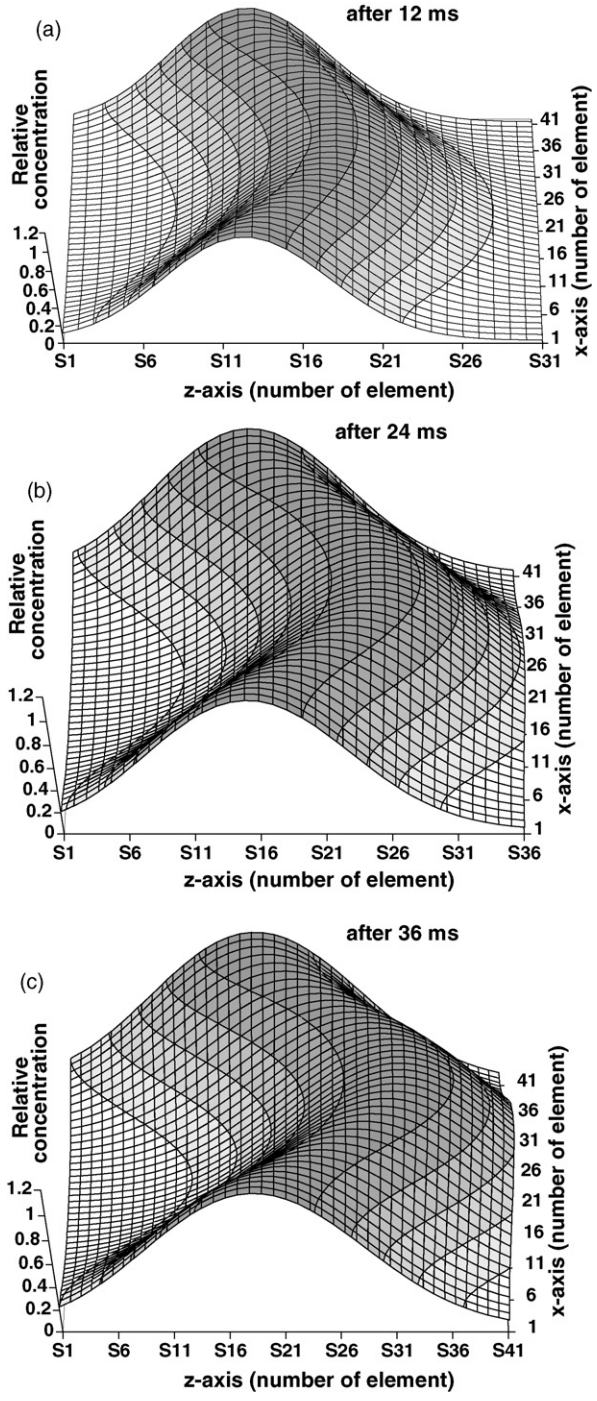

Fig. 1 – Concentration dispersion in a 40 μm high rectangular channel at a flow velocity v_0 of 0.04 cm s^{-1} after time periods of 12 ms (a), 24 ms (b), and 36 ms (c). Computer-simulated concentration profiles are shown as a function of the height coordinate x and the length coordinate z. The element numbers correspond to n for the x-axis, and to $p - 10$ for the z-axis, respectively. From (a) to (c), the length axis is scaled down by a factor proportional to $\sqrt{t}$. Concentrations are given in units of the respective maximum value found for the average concentration c_{av} in x-direction.

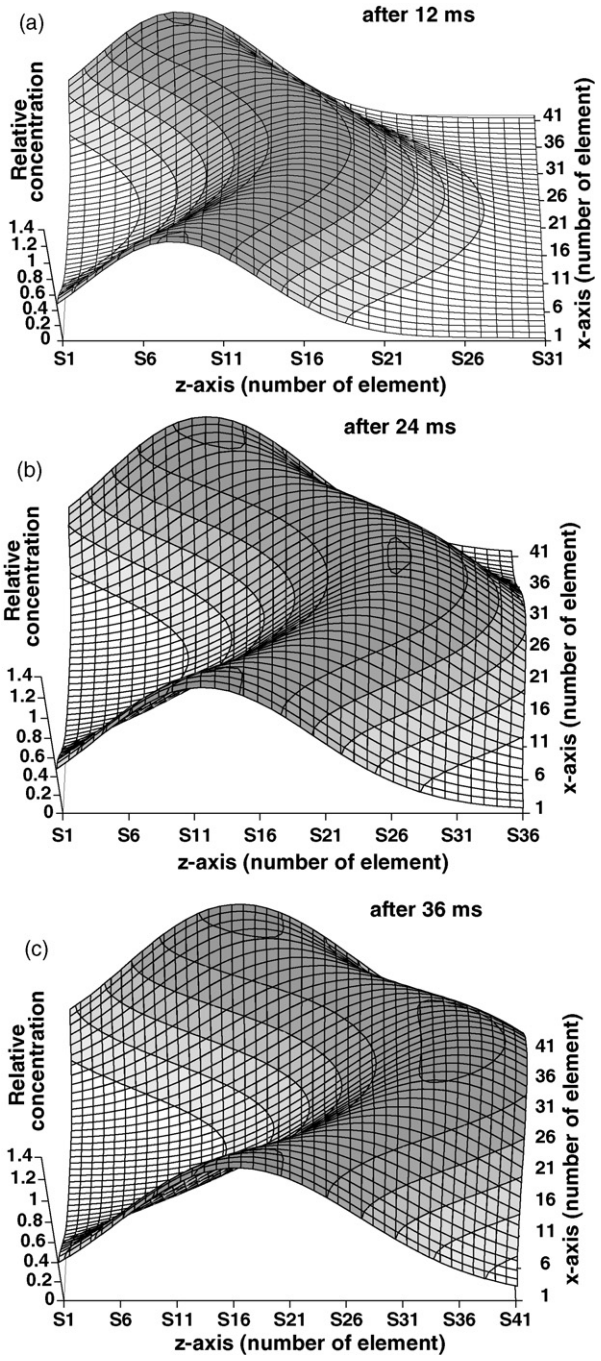

Fig. 2 – Concentration dispersion in a 40 μm high rectangular channel at a flow velocity v_0 of 0.06 cm s^{-1} after time periods of 12 ms (a), 24 ms (b), and 36 ms (c). Computer simulations as in Fig. 1, except that here the element numbers on the z-axis correspond to $p - 15$.

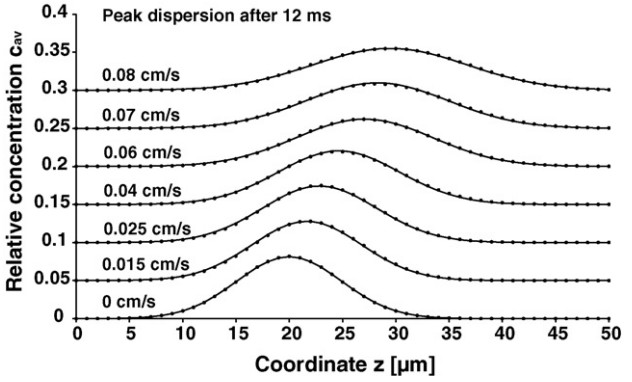

Fig. 3 – Peak profiles in a 40 μm high rectangular channel after 12 ms at a flow velocity v_0 of 0, 0.015, 0.025, 0.04, 0.06, 0.07, and 0.08 cm s^{-1}, respectively. At t = 0 the solute was in the elements at a distance of 20 μm on the z-axis. Points: concentrations c_{av} obtained from computer simulations, given in units of the initial concentration c_{in}. Lines: Gaussian curves fitted from Eq. (9).

ranging from 12 to 36 ms. In Figs. 1 and 2, the z-coordinate was scaled down by a factor proportional to $\sqrt{t}$ in order to compensate for the expected peak broadening with increasing time (see Eq. (13)). Actually, this leads to a roughly constant shape of the concentration distribution. It is surprising that the basic details of the peak profile appear to be preformed after only a few milliseconds. However, the peak evolution is still proceeding after this time period since Figs. 1 and 2 indicate a further increase of the scaled peak width. The reason is that a diffusion time $t_d = h^2/2D$ [42] of about 1 s is expected for a perfect lateral equilibration in the channel. Such long virtual experiments would exceed the capacity of the present numerical calculations. Nevertheless, the computer simulations can be used to extrapolate the parameters of the long-term behavior very exactly, as shown below.

The concentration profiles for the frontal elements in Figs. 1 and 2 clearly follow a Gaussian distribution curve. Eqs. (9) and (16) predict an analogous profile for the average concentrations at different locations z. This is confirmed by the results of computer simulations in Fig. 3. The shown peak profiles were determined in virtual experiments of 12 ms duration at flow velocities v_0 ranging from 0.015 to 0.08 cm s^{-1}. The data points obtained by the finite-element computer simulation are perfectly fitted by solid curves according to Eq. (9). Similar excellent correlations were found for the peak pro-

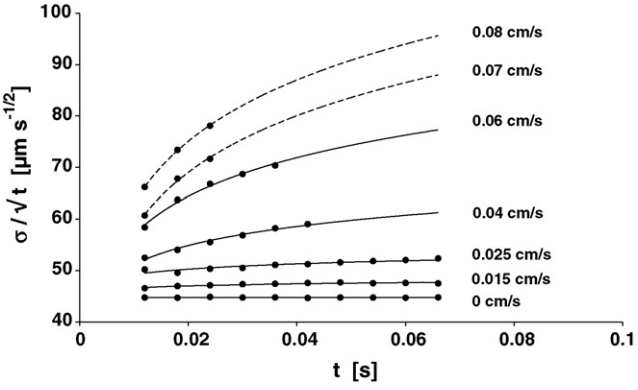

Fig. 4 – Values of the scaled peak half-width ($\sigma/\sqrt{t}$) as a function of the time t at a flow velocity v_0 of 0, 0.015, 0.025, 0.04, 0.06, 0.07, and 0.08 cm s^{-1}, respectively. Points: Data obtained from computer simulations as in Fig. 3. Lines: Fitted trendlines.

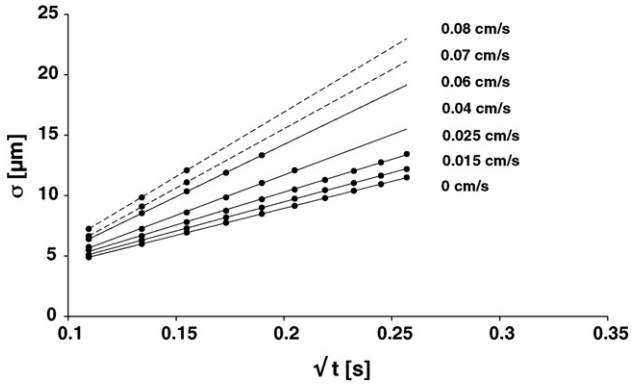

Fig. 5 – Values of the peak half-width σ as a function of $\sqrt{t}$ at a flow velocity v_0 of 0, 0.015, 0.025, 0.04, 0.06, 0.07, and 0.08 cm s^{-1}, respectively. Points: Computer-simulated results from Fig. 4. Lines: Regressions from Eq. (17) with the parameters of Table 1.

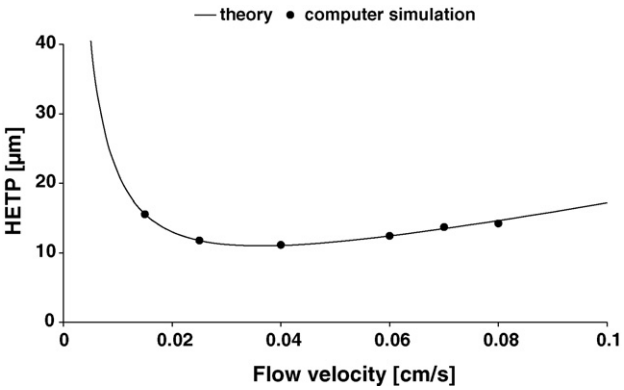

Fig. 6 – Extrapolated HETP value for sufficiently long times as a function of the flow velocity v_0. Points: Values a^2/v_0 obtained from Table 1. Line: Theoretical curve according to Eq. (14).

files after longer time intervals. At high velocities, however, the accessible time range was limited by the fixed size of the channel section that was studied by the present numerical procedure. Therefore, a maximum period of 24 ms was taken as reliable for the virtual experiments at flow velocities of 0.07 and 0.08 cm s^{-1}.

The curve fits to the various computer-simulated peaks allowed it to determine the observed standard half-width σ as a function of the time. This procedure was carried out for different flow velocities, and also for a purely diffusion-controlled system with $v_0 = 0$. Fig. 4 shows the time-scaled results, $\sigma/\sqrt{t}$, as a function of t. These values are found to approach a constant level, as predicted by Eq. (13), after a certain initial period. The duration of the initial equilibration processes obviously depends on the actual flow velocity. It ranges from a few milliseconds for cases where longitudinal diffusion predominates ($v_0 \leq 0.025$ cm s^{-1}) to >0.1 s for cases where convection-induced dispersion becomes decisive ($v_0 \geq 0.06$ cm s^{-1}, see Fig. 4). However, the long-term behavior of solute peaks can be perfectly predicted even from the data collected during this early period, as demonstrated below.

In Fig. 5, the values σ obtained from the computer simulations are plotted as a function of $\sqrt{t}$. Evidently, a strictly linear relationship according to Eq. (17) is exhibited in all cases, the regression parameters a and b being summarized in Table 1:

$$\sigma = a\sqrt{t} + b \tag{17}$$

The linear dependence of σ on $\sqrt{t}$ is in accordance with Eq. (13). On the other hand, the intercept b of the linear regression lines in Fig. 5 is different from zero and turns out to be negative, except for the pure diffusion case (see Table 1). This behavior can be explained by the initial delay in the lateral equilibration processes that are involved in the final peak evolution. A negative intercept b would at least corroborate such an interpretation.

Definitely, the regression lines in Fig. 5 approach the theoretical values for the peak half-width σ when the time period is sufficiently long, that is, for a $\sqrt{t} \gg b$. This important fact is evident from Table 1 where a nearly perfect correlation is found between the regression slopes a and the respective quantities calculated from Eq. (13). In Fig. 6, the extrapolated long-term results for HETP are compared with the corresponding curve from Eq. (14). Evidently, an excellent agreement between virtual experiment and theory at different flow velocities is documented. From Eq. (14) a minimal HETP value of 11.05 µm is quoted for $v_0 = 0.036$ cm s^{-1}, which is nearly identical to the simulated value of 11.18 µm for 0.04 cm s^{-1}. The convincing results in Fig. 6 demonstrate the suitability of computer simulations for investigating the peak evolution in microfluidic

Table 1 – Linear regression parameters for the σ values in Fig. 5

Flow velocity v_0 (cm s^{-1})	Slope a[a] (µm s$^{-1/2}$)	Intercept b[a] (µm)	Expected a[b] (µm s$^{-1/2}$)
0	44.74	0	44.72
0.015	48.34	−0.180	48.40
0.025	54.35	−0.590	54.34
0.04	66.89	−1.674	66.62
0.06	86.51	−3.067	86.52
0.07	98.12	−4.087	97.30
0.08	106.85	−4.464	108.41

[a] Values a and b based on Eq. (17).

[b] Values $\sqrt{(2D^*)} = \sqrt{(2D + v_0^2h^2/105D)}$ according to Eq. (13).

channels. Finally, they also confirm the strict validity of the fundamental HETP relationship for the studied system.

5. Conclusions

Computer simulations were performed to study the dynamics of peak formation in rectangular microfluidic channels. The underlying diffusion and convection processes were modeled by finite-element techniques. Two-dimensional concentration dispersions were determined and analyzed for the case of sufficiently wide channels. Such virtual experiments generally allowed it to explore the time-dependent performance of microfluidic channels. The extrapolated long-term behavior was in excellent agreement with theoretical predictions. For this purpose the theory of open-channel HPLC was applied.

REFERENCES

[1] G.M. Whitesides, Nature (London) 442 (2006) 368.
[2] B. Bhushan (Ed.), Springer Handbook of Nanotechnology, second ed., Springer, Berlin, 2007, p. 523.
[3] A. Manz, N. Graber, H.M. Widmer, Sens. Actuators B1 (1990) 244.
[4] B.H. van der Schoot, S. Jeanneret, A. van den Berg, N.F. de Rooij, Anal. Methods Instrum. 1 (1993) 38.
[5] D. Janasek, J. Franzke, A. Manz, Nature (London) 442 (2006) 374.
[6] H. Nakanishi, Chem. Sensors (Denki Kagakkai Kagaku Sensa Kenkyukai Japan) 22 (2006) 8.
[7] G. Chen, Y. Lin, J. Wang, Curr. Anal. Chem. 2 (2006) 43.
[8] Y. Sun, Y.C. Kwok, Anal. Chim. Acta 556 (2006) 80.
[9] J.G.E. Gardeniers, A. van den Berg, Anal. Bioanal. Chem. 378 (2004) 1700.
[10] O.T. Guenat, W.E. Morf, B.H. van der Schoot, N.F. de Rooij, Anal. Chim. Acta 361 (1998) 261.
[11] O.T. Guenat, B.H. van der Schoot, W.E. Morf, N.F. de Rooij, Anal. Chem. 72 (2000) 1585.
[12] J.C.T. Eijkel, A. van den Berg, Microfluid. Nanofluid. 1 (2005) 249.
[13] C.H. Ahn, J.-W. Choi, in: B. Bhushan (Ed.), Springer Handbook of Nanotechnology, second ed., Springer, Berlin, 2007, p. 523.
[14] A. Manz, W. Simon, Anal. Chem. 59 (1987) 74.
[15] G. Taylor, Proc. R. Soc. (Lond.) A219 (1953) 186.
[16] M.J.E. Golay, in: D.H. Desty (Ed.), Gas Chromatography (Proc. Symposium, Amsterdam), Butterworths, London, 1958, p. 36.
[17] M.J.E. Golay, J.G. Atwood, J. Chromatogr. 186 (1979) 353.
[18] J.J. van Deemter, F.J. Zuiderweg, A. Klinkenberg, Chem. Eng. Sci. 5 (1956) 271.
[19] J.C. Giddings, Anal. Chem. 35 (1963) 2215.
[20] J.C. Giddings, Dynamics of Chromatography Part 1, M. Dekker, New York, 1965.
[21] J.C. Giddings, J.P. Chang, M.N. Myers, J.M. Davis, K.D. Caldwell, J. Chromatogr. 255 (1983) 359.
[22] J.H. Knox, M.T. Gilbert, J. Chromatogr. 186 (1979) 405.
[23] J.T. Vanderslice, A.G. Rosenfeld, G.R. Beecher, Anal. Chim. Acta 179 (1986) 119.
[24] D.O. Hancock, C.N. Renn, R.E. Synovec, Anal. Chem. 62 (1990) 2441.
[25] G.E. Spangler, Anal. Chem. 78 (2006) 5205.
[26] G.E. Spangler, J. Microcolumn Sep. 13 (2001) 285.
[27] G.E. Spangler, Anal. Chem. 70 (1998) 4805.
[28] D. Liang, Q. Peng, K. Mitchelson, X. Guan, W. Xing, J. Cheng, Lab Chip 7 (2007) 1062.
[29] D. Dutta, D.T. Leighton Jr., Anal. Chem. 75 (2003) 57.
[30] H. Poppe, J. Chromatogr. A 948 (2002) 3.
[31] G. Desmet, G.V. Baron, J. Chromatogr. A 946 (2002) 51.
[32] M.J.E. Golay, J. Chromatogr. 216 (1981) 1.
[33] H. Ahn, S. Brandani, AJChE J. 51 (2005) 1980.
[34] X. Bai, J. Josserand, H. Jensen, J.S. Rossier, H.H. Girault, Anal. Chem. 74 (2002) 6205.
[35] X. Zhang, F.E. Regnier, J. Chromatogr. A 869 (2000) 319.
[36] E. Toshev, Kh. Boyadjiev, Hung. J. Ind. Chem. 22 (1994) 81.
[37] S.-C. Pai, Y.-H. Lai, L.-Y. Chiao, T. Yu, J. Chromatogr. A 1139 (2007) 109.
[38] R.J. Cornish, Proc. R. Soc. Lond. A120 (1928) 691.
[39] S. Böhm, W. Olthuis, P. Bergveld, Proceedings of the Transducers, Sendai, Japan, 1999, p. 880.
[40] W.E. Morf, O.T. Guenat, N.F. de Rooij, Sens. Actuators B72 (2001) 266.
[41] C. Gerthsen, H.O. Kneser, Physik, 10th ed., Springer, Berlin, 1969.
[42] J. Crank, The Mathematics of Diffusion, second ed., Clarendon Press, Oxford, UK, 1975.
[43] W.E. Morf, M. Koudelka-Hep, N.F. de Rooij, J. Electroanal. Chem. 590 (2006) 47.
[44] W.E. Morf, E. Pretsch, N.F. de Rooij, J. Electroanal. Chem. 602 (2007) 43.
[45] W.E. Morf, E. Pretsch, N.F. de Rooij, J. Electroanal. Chem. 614 (2008) 15.